EES Solar

PERSPECTIVE

View Article Online
View Journal | View Issue

Check for updates

Cite this: *EES Sol.*, 2026, **2**, 315

Perovskite/perovskite/silicon triple-junction solar cells: progress, challenges, and perspectives

Fuzong Xu, * Anand S. Subbiah, Ahmed Ali Said, Thomas Allen and Stefaan De Wolf *

Received 19th December 2025
Accepted 3rd February 2026

DOI: 10.1039/d5el00213c

rsc.li/EESSolar

Perovskite/perovskite/silicon triple-junction solar cells are a rapidly developing technology in multi-junction photovoltaics and metal halide perovskite research, driven by their potential to exceed the power conversion efficiency (PCE) limits of current technologies. Despite this promise, their performance and operational stability remain notably behind their two-junction counterparts. In this perspective, we provide a comprehensive analysis of this complex device architecture from three key perspectives, by focusing on the device configuration and the distinct roles of the perovskite top and middle cells. We highlight recent progress, identify the fundamental bottlenecks, and outline key research directions that could unlock significant improvements in both PCE and long-term stability.

Broader context

Perovskite/perovskite/silicon triple-junction solar cells have emerged as a promising next-generation photovoltaic device architecture, owing to their exceptionally high theoretical power conversion efficiency and high open-circuit voltage. However, as the technology is still in its infancy, current devices suffer from insufficient efficiency and stability, limiting their practical deployment. This perspective offers a comprehensive summary of recent advances in triple-junction solar cells, focusing on device designs, key material choices and integration strategies. Based on the authors' research experience, this article identifies critical scientific and technological challenges, highlights promising research directions, and discusses potential solutions to accelerate progress. By consolidating the latest developments and offering targeted guidance, this perspective aims to serve as a valuable reference for researchers entering the field. It is expected to promote faster development of perovskite/perovskite/silicon triple-junction solar cells and support their transition from laboratory prototypes to high-performance, stable, and scalable photovoltaic technologies. As interest in multi-junction strategies continues to grow, this review provides timely insight into one of the most rapidly evolving directions in solar energy research.

Introduction

Achieving higher power conversion efficiencies (PCEs) has long been a central objective in the development of solar cells as a key solution in the energy transition. For single-junction (1-J) solar cells, the theoretical PCE limit under standard test conditions (STC, 1 Sun AM 1.5G spectrum, 25 °C); is approximately 33.7% under the detailed balance model, constrained primarily by two intrinsic loss mechanisms: transmission losses, where sub-bandgap photons are not absorbed, and thermalization losses, where the excess energy of high-energy photons is dissipated as heat.[1,2] Tandem solar cells offer a promising and realistic route to mitigate these losses by incorporating multiple absorbers with different bandgaps into a single device. In such architectures, wider-bandgap absorbers, located at the light-incident side, help reduce thermalization losses, while narrower-bandgap absorbers underneath capture photons that would otherwise pass through without electron–hole generation.[3–7] This design enables a significantly higher theoretical Shockley–Queisser (S–Q) efficiency limit, reaching up to 86.8% under concentrated illumination and around 68.2% under STC, assuming an unlimited number of junctions can be incorporated into the device.[8]

Among various tandem architectures, those combining perovskites and crystalline silicon (c-Si) have received significant attention. Their appeal stems from several distinct advantages, including the low material cost of both perovskite and c-Si, the well-established status of c-Si in the PV manufacturing industry, the highly tunable bandgap of perovskite materials that is well suited for top-cell integration, and the excellent optoelectronic properties of perovskites.[9–14] Monolithic perovskite/Si two-junction (2-J) tandem solar cells have achieved certified PCEs approaching 35% under STC, surpassing the S–Q limit of any single-junction solar cell.[15] These advances underscore both the performance advantage of tandem designs and the synergistic integration of perovskite and Si sub-cells. Building on this foundation, perovskite/perovskite/Si triple-junction (3-J) tandem solar cells, with Si as the bottom layer for long-wavelength absorption and two perovskite layers as the middle and top sub-cells for short-

Center for Renewable Energy and Storage Technologies (CREST), King Abdullah University of Science and Technology (KAUST), Thuwal, Kingdom of Saudi Arabia. E-mail: fuzong.xu@kaust.edu.sa; stefaan.dewolf@kaust.edu.sa

Open Access Article. Published on 04 February 2026. Downloaded on 5/20/2026 12:36:25 AM. This article is licensed under a Creative Commons Attribution 3.0 Unported Licence.

Open Access Article. Published on 04 February 2026. Downloaded on 5/20/2026 12:36:25 AM. This article is licensed under a Creative Commons Attribution 3.0 Unported Licence.

wavelength absorption, offer a higher theoretical PCE ceiling of 49.3% under STC. These architectures hold great promises for further improving efficiency beyond the limit of 2-J counterparts. Yet, although the theoretical efficiency increases with additional junctions, the gain typically exhibits diminishing returns, *i.e.*, the incremental efficiency benefit becomes smaller with each added junction, whereas device complexity and integration losses tend to increase.[8] Nevertheless, record multi-junction photovoltaics in GaAs-based technology are commonly realized in 3-J configurations,[16] suggesting that 3-J devices can represent a practical balance point between efficiency potential and device complexity and cost.

Despite this potential, the development of 3-J tandem solar cells remains in its early stages with PCEs still below their 2-J counterparts. Key challenges include the increased structural complexity, the need for bandgap-optimized and mutually compatible perovskite layers, and the limited adaptability of conventional device fabrication techniques. Although the field is attracting growing interest and the number of related studies is rising, a comprehensive and systematic discussion of current progress, device strategies, and material bottlenecks remains lacking. In this context, it is both timely and necessary to critically assess recent developments and highlight key directions for advancing perovskite/perovskite/Si 3-J solar cells.

Device architecture of perovskite/perovskite/Si tandem solar cells

For advanced tandem solar cell architectures, the initial design priority is to identify the optimal bandgaps and absorber thicknesses to achieve current matching across all sub-cells. This requirement is especially stringent in monolithic devices, where sub-cells are connected in series and the device current is dictated by the lowest-performing sub-cell. As the operating voltage increases with each additional junction, maintaining precise current matching at maximum power point conditions is crucial to prevent performance losses.[8,17]

According to detailed-balance calculations that include the effects of luminescent coupling between sub-cells and back reflection in the Si bottom cell (Fig. 1a), the theoretical maximum PCE of perovskite/perovskite/Si 3-J solar cells can reach 49.3% at STC. This configuration corresponds to an open-circuit voltage (V_{oc}) of 3.75 V, a fill factor (FF) of 90.3%, and a short-circuit current density (J_{sc}) of 14.6 mA cm^{-2}, where the top (Top) and middle (Mid) perovskite sub-cells have ideal bandgaps of 2.001 eV and 1.493 eV, respectively. These bandgaps fall within the reported ranges of perovskite materials, which span approximately from 1.22 eV to 3.02 eV.[6,18–22]

Nevertheless, to come close to a realistic PCE estimate and practical design rules for the bandgaps, one must account for optical losses. A representative architecture of the 3-J tandem structure is shown schematically in Fig. 1b. When optical losses are considered but electronic losses are neglected, the optimal bandgaps of the perovskite sub-cells shift toward slightly narrower values. This adjustment compensates for optical attenuation caused by ancillary layers such as transparent electrodes (usually transparent conductive oxides, TCOs), electron and hole transport layers (ETLs and HTLs). While the c-Si bottom sub-cell's bandgap is fixed at 1.12 eV at 25 °C, simulations have shown that the top and middle perovskite layers require narrower bandgaps than in the ideal case, typically around 1.95 eV and 1.44 eV, respectively.[23] It should be noted, however, that these optimal values can vary depending on the specific device architecture and optical stack as well as actual deployment conditions, which may imply temperature and spectral deviations from STC.

As with other tandem designs, perovskite/perovskite/Si 3-J solar cells can be implemented in either monolithic or mechanically stacked configurations (Fig. 1b). In either case, the preferred Si bottom cell is based on state-of-the-art technology featuring passivating contacts, such as silicon heterojunction cells. In monolithic designs, adjacent sub-cells are interconnected through a recombination junction that enables efficient charge transfer between the sub-cells in a series connection.[33–35] This architecture typically enables a higher PCE compared to the mechanical stacked devices, due to reduced optical losses and a more compact design. Currently, among the most critical structural elements in monolithic 3-J devices is the interconnecting recombination layer between the top- and mid-cell perovskite photo-absorbers. The state-of-the-art approach relies on metal-oxide films, contrasting with the typical 1 nm thin Au-based recombination layers used in perovskite/perovskite 2-J tandem solar cells, as the latter would induce substantial parasitic optical absorption, particularly detrimental to the mid-cell, despite their favorable electrical properties.[26] Thus far, all perovskite/perovskite/Si 3-J solar cells, developed in the wake of high-efficiency perovskite/Si devices, employ a p–i–n configuration involving atomic layer deposited (ALD) SnO_x in the interconnection structure between the top and mid sub-cells. Here, SnO_x mainly serves as a buffer layer compatible with the underlying C_{60} ETL and protecting it from sputtering damage of an overlying transparent electrode, usually indium zinc oxide (IZO) or indium tin oxide (ITO), drawing inspiration from the top contact as developed for perovskite/Si 2-J counterparts. Nonetheless, the mechanical fragility of these ultrathin SnO_x interlayers often poses a risk of failure during subsequent solution-based fabrication processes of the top-cell. A temporary workaround solution has been to increase the SnO_x thickness to improve mechanical durability, but this inevitably leads to optical and electrical losses.[26] Therefore, the development of interconnect layers with improved mechanical properties, without compromising optical transparency and electrical performance, is essential for the advancement of monolithic 3-J devices. Potential pathways to this end include employing Al_2O_3-based metal oxides, deposited as dense films by low-temperature ALD, as buffer layers to improve the mechanical robustness of the interconnection structure without compromising integration compatibility. Beyond developing mechanically robust interconnection structures, solution-free processing routes for the subsequent device layers (*e.g.* through chemical or physical vapor deposition), including the top-cell perovskite photoabsorber, may also

© 2026 The Author(s). Published by the Royal Society of Chemistry

Open Access Article. Published on 04 February 2026. Downloaded on 5/20/2026 12:36:25 AM.
This article is licensed under a Creative Commons Attribution 3.0 Unported Licence.

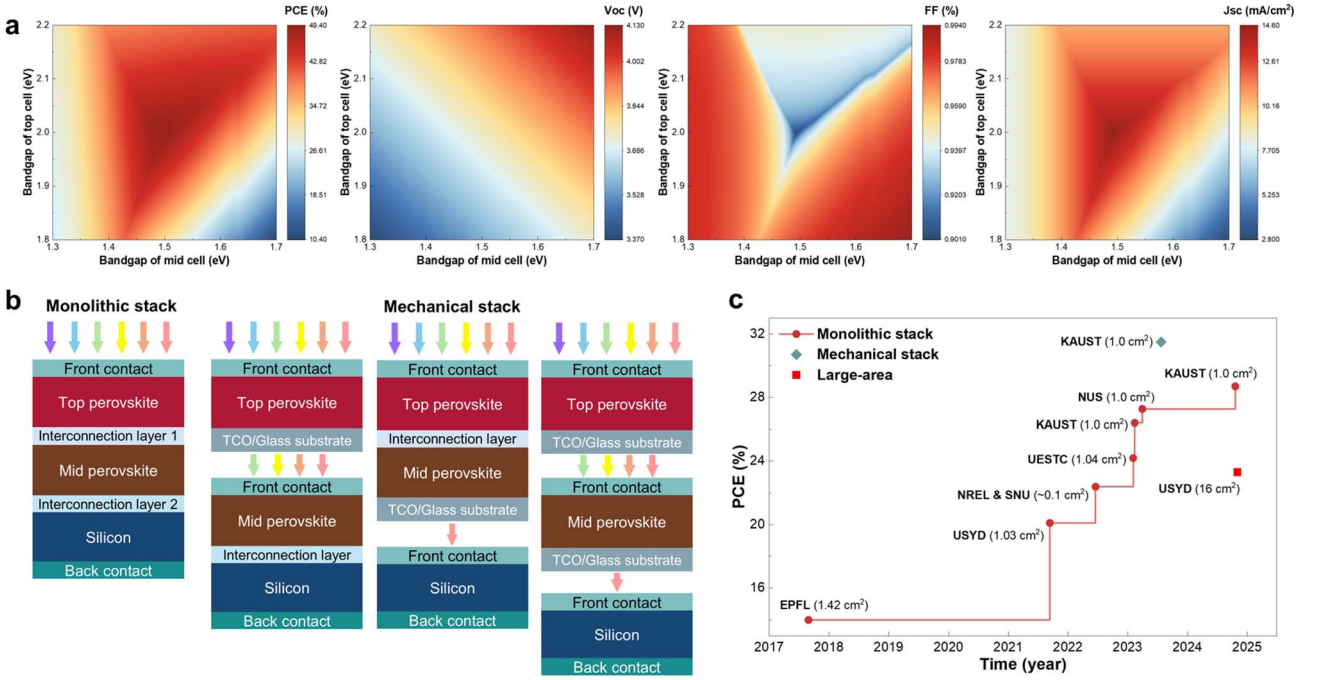

Fig. 1 (a) Simulated Shockley–Queisser (S–Q) limits for the power conversion efficiency (PCE), open-circuit voltage (V_{oc}), fill factor (FF), and short-circuit current density (J_{sc}) of perovskite/perovskite/Si 3-J tandem solar cells as a function of the bandgaps of the top and mid perovskite sub-cells; (b) schematic illustration of perovskite/perovskite/Si 3-J device architectures: monolithic *versus* mechanically stacked configurations; (c) summary of the highest reported efficiencies of perovskite/perovskite/Si 3-J solar cells based on different stacked architectures, including monolithic, mechanically stacked, and large-area module formats.[24–32]

mitigate solvent-related disturbance during monolithic integration.

In contrast, mechanically stacked tandem cells allow for greater flexibility in bandgap selection because the sub-cells operate independently and can be electrically connected in parallel. This removes the strict requirement for current matching. Moreover, the modular nature of mechanical stacking ensures that degradation in one sub-cell does not necessarily render the entire device nonfunctional. However, this device architecture suffers from increased optical losses due to its reliance on additional transparent substrates, electrodes, and the multiple interfaces where light transitions between media. Although optical index-matching materials can mitigate some of these losses, the overall PCE remains limited by suboptimal light management.

The development trajectory of 3-J tandems is illustrated in Fig. 1c. From their initial demonstration in 2018 through early 2024, most devices exhibited relatively low PCEs.[31] A breakthrough occurred in early 2024, when the PCE of a monolithic 3-J device first exceeded that of contemporary 1-J perovskite cells and approached parity with state-of-the-art perovskite/perovskite 2-J solar cells.[26] The highest reported PCE for monolithic 3-J devices now stands at 28.7% for a 1 cm^2 device.[24] In terms of scaled devices, the best results to date for a monolithic 3-J tandem is a PCE 23.3% over an active area of 16 cm^2.[32]

Even more so than for 2-J solar cells, the complex structure of 3-J devices requires careful optimization of optical and electrical design, which currently favor mechanically stacked architectures, where multiple implementations are possible. Yet, the most practical ones will rather be in a four than a six-terminal layout. For instance, to date, the highest reported PCE for 3-J tandem solar cells has been achieved for a four-terminal 3-J tandem, consisting of a monolithic perovskite/Si tandem, onto which an additional, wider bandgap perovskite cell is mechanically stacked, reaching combined a PCE of 31.5%.[28]

Top perovskite sub-cell: requirements, challenges, and strategies

Simulation results indicate that the optimal bandgap for the top-cell perovskite is approximately 2.0 eV (Fig. 1a). However, during fabrication, it is often advantageous to employ thinner perovskite layers, which can justify the use of a slightly lower bandgap. This trade-off sacrifices some of the V_{oc} and FF in exchange for improved film processability and easier current matching. Therefore, the precise bandgap choice depends strongly on the deposition method and the target layer thickness.

A survey of reported devices reveals that the bandgap of top-cell perovskite layers typically ranges from 1.8 to 2.0 eV (Fig. 2a). The corresponding device parameters, V_{oc}, FF, and V_{oc} × FF, vary with composition. Because J_{sc} is often tuned through thickness optimization, it is excluded from direct comparison. Currently, all high-performing top-cells employ organic–inorganic hybrid perovskites, owing to their superior optoelectronic

© 2026 The Author(s). Published by the Royal Society of Chemistry

Open Access Article. Published on 04 February 2026. Downloaded on 5/20/2026 12:36:25 AM.
This article is licensed under a Creative Commons Attribution 3.0 Unported Licence.

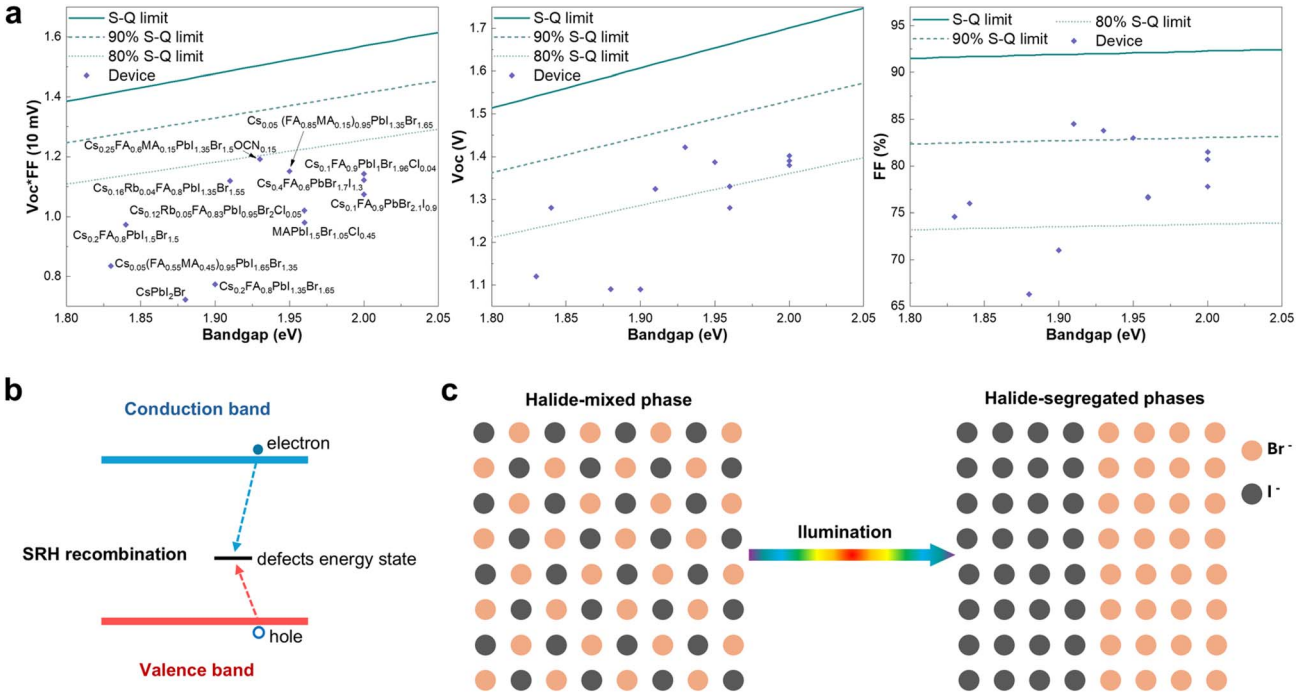

Fig. 2 (a) Summary of reported top-cell performance parameters in perovskite/perovskite/Si 3-J solar cells, including V_{oc}, FF, and the combined $V_{oc} \times$ FF, alongside the corresponding perovskite compositions and optical bandgaps;[24–32,36–40] (b) schematic illustration of Shockley–Read–Hall (SRH) nonradiative recombination, a key efficiency-limiting factor in top perovskites; (c) illustration of illumination-induced halide phase segregation, a persistent instability issue in I–Br mixed-halide perovskites used as top absorbers.

properties and favorable processing compatibility.[26] Their relatively low annealing temperatures render them more compatible with underlying sub-cells, whereas fully inorganic perovskites require high-temperature annealing due to solvent-mediated crystallization, which can damage previously deposited absorbers or organic charge transport layers.[41–44] Despite these merits, ultra-wide-bandgap perovskites still suffer from two fundamental problems: significant PCE losses and pronounced photo-instability.

When benchmarked against the S–Q limit, certain compositions achieve V_{oc} values exceeding 80% of their theoretical maximum and FF values surpassing 90% (Fig. 2a). However, their combined $V_{oc} \times$ FF product remains below 80% of the S–Q limit, considerably lower than the >90% values observed in state-of-the-art high-PCE 1-J perovskite solar cells.[1,15] This shortfall arises from intrinsic limitations of ultra-wide-bandgap perovskites. As the bandgap widens, formerly shallow traps become deeper, promoting Shockley–Read–Hall (SRH) nonradiative recombination (Fig. 2b). Moreover, the wider bandgap can cause unfavorable band alignment with adjacent ETLs and HTLs, further hindering carrier extraction.[22,45] Achieving wide bandgaps also requires a highed Br^- content to partially replace I^-, often exceeding 50%, which triggers light-induced phase segregation where mixed halides separate into I-rich and Br-rich domains under illumination (Fig. 2c). This segregation severely compromises device stability.[46–50] Combined, deep-level defects and halide segregation constitute the core scientific challenges for the top perovskite layers.

Recent progress has focused on mitigating these issues through both grain-scale and lattice-scale engineering. Because phase segregation frequently originates at grain boundaries where defects accumulate, some research aims to reduce the grain boundary density and passivate interfacial traps, yielding notable improvements in PCE and stability.[26,27] At the lattice level, compositional modifications help relieve strain and suppress defect formation. For instance, cyanate ions (OCN^-) have been introduced to partially replace halides, alleviating lattice strain, while 3-ammoniumpropionic acid ($3A^+$) has been used to substitute FA^+, forming additional lattice bonds. This approach suppresses Schottky defect formation and increases the activation barrier for phase transitions, thereby reducing phase segregation and enhancing optoelectronic performance.[24,25] Continued efforts to stabilize ultra-wide-bandgap perovskites *via* defect management and composition-driven thermodynamic adjustment, enhance carrier extraction, and minimize nonradiative losses will be crucial for advancing the top-cell efficiency and reliability in 3-J tandems.

Middle perovskite sub-cell: requirements, challenges, and strategies

As illustrated in Fig. 3a, simulations based on the S–Q considerations indicate that the optimal bandgap for the mid-cell is about 1.49 eV. In real devices, the ideal bandgap is often slightly smaller to account for optical losses from parasitic absorption

© 2026 The Author(s). Published by the Royal Society of Chemistry

Open Access Article. Published on 04 February 2026. Downloaded on 5/20/2026 12:36:25 AM.
This article is licensed under a Creative Commons Attribution 3.0 Unported Licence.

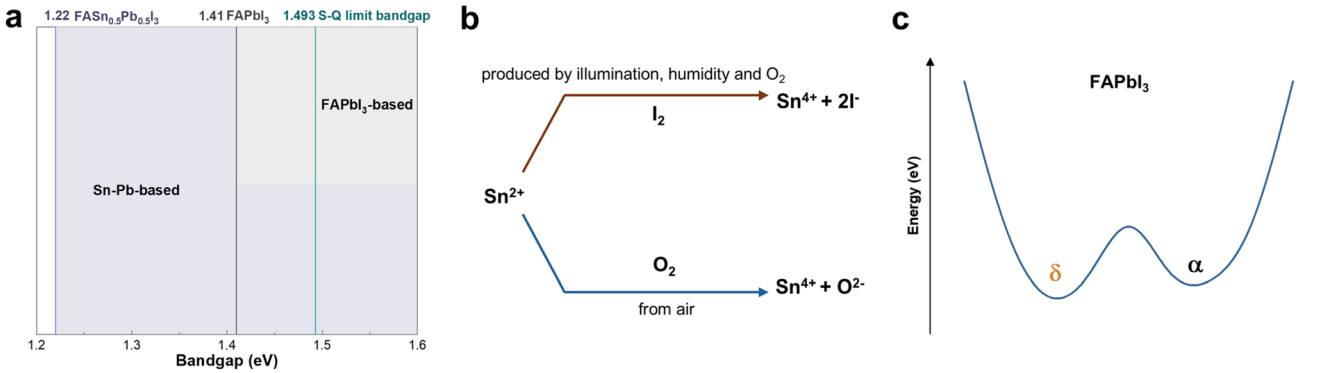

Fig. 3 (a) Summary and comparison of Sn–Pb-based and $FAPbI_3$-based perovskite compositions explored as mid sub-cell absorbers in triple-junction solar cells, alongside their corresponding experimental bandgaps and the theoretically optimal bandgap range for mid-cells; (b) schematic of the degradation pathway in Sn–Pb perovskites, highlighting the oxidation of Sn^{2+} to Sn^{4+} as a major instability mechanism; (c) illustration of the thermodynamic instability of the black α-phase of $FAPbI_3$, which tends to transform into the yellow δ-phase under ambient conditions.

in transport layers and incomplete absorption in thin films. Consequently, appropriate compositions generally exhibit bandgaps wider than 1.41 eV for $FAPbI_3$ perovskites and >1.22 eV for Sn–Pb alloys.[51–53]

Each system presents distinct difficulties. Sn–Pb perovskites, in principle, can offer a nearly ideal bandgap for the mid-cells (Fig. 3a), yet their practical application is limited by chemical instability, particularly due to the oxidation of Sn^{2+} to Sn^{4+} (Fig. 3b). Although O_2-induced oxidation can be mitigated through robust encapsulation, I_2 is a more persistent oxidant. Because I_2 can also form under illumination even in inert environments, apart from being produced by the O_2 and H_2O in air, its completely suppression remains challenging. Stabilizing Sn^{2+} against oxidation is therefore a central research focus.[54–57] Encouragingly, substantial advances have been achieved for perovskite/perovskite 2-J solar cells employing ~1.22 eV Sn–Pb perovskite bottom cells, providing valuable insight for 3-J designs.[6,21,58,59]

Given these constraints, most reported 3-J devices currently avoid the use of Sn-based perovskites as the middle absorber, rather utilizing $FAPbI_3$-based perovskites. Compared with Sn–Pb counterparts, $FAPbI_3$ offers superior ambient phase stability and benefits from the extensive understanding gained from high efficiency 1-J devices.[13,14] Nevertheless, several intrinsic challenges are associated with this choice. The claimed ~1.41 eV bandgap of this material corresponds to bulk single crystals (Fig. 3a), while thin films with nanoscale grains typically exhibit blue shifted gaps (>1.45 eV) due to quantum confinement and strain.[53,60–62] This shift decreases photocurrent generation. To minimize such losses, the material must remain nearly stoichiometric $FAPbI_3$. However, stoichiometric $FAPbI_3$ is prone to phase instabilities because its black photoactive α-phase is thermodynamically metastable and has a higher free energy than the yellow photoinactive δ-phase (Fig. 3c). Consequently, spontaneous α → δ transition often occurs under ambient conditions, severely degrading device performance.[13,63–65] In 1-J cells, this issue is typically mitigated by partially substituting FA^+ with Cs^+ or MA^+ and I^- with Br^-. Although this improves phase stability, it also widens the bandgap beyond ~1.55 eV, which causes the current imbalance in 3-J tandem solar cells.[24] Therefore, enhancing α-phase stability without significantly altering the bandgap remains a crucial goal.

Only a few studies have directly addressed this challenge for 3-J tandems. Recent reports show that lattice-stiffening strategies, such as suppressing vacancy formation and increasing the phase-transition energy barrier, can simultaneously enhance device stability and PCE. Beyond phase stability, optical absorption also imposes constraints: because the bandgap of $FAPbI_3$ films (>1.45 eV) is already near the S–Q optimum, complete photon harvesting demands unusually thick layers. Such films must combine strong absorption with efficient carrier extraction, posing fabrication challenges. Reproducibly depositing thick, high-crystallinity, low-defect films is therefore vital. In practice, $FAPbI_3$-based mid-cells typically require >2 μm thickness for textured configurations and >1.5 μm for planar designs.[24] However, thick mid-cell perovskite photo-absorbers are often deposited from high-concentration precursor solutions, which can accelerate crystallization and increase the difficulty of achieving reproducible, high-quality thick films. Moreover, crystallization of the mid-cell perovskite on textured or non-planar underlying device stacks is also a critical challenge; however, as the underlying mechanisms and mitigation strategies largely overlap with those extensively discussed for perovskite/Si 2-J tandems, we do not elaborate on this topic here.

Summary and outlook

As discussed throughout this perspective, both the perovskite/perovskite/silicon 3-J and perovskite/silicon 2-J tandem configurations are built onto an efficient Si bottom-cell. To date, the performance limitations of 3-J devices have not originated from the used Si bottom-cell. Instead, the primary bottlenecks are concentrated in the complex device configuration, in particular the recombination junction between top- and mid-cell, and the

Open Access Article. Published on 04 February 2026. Downloaded on 5/20/2026 12:36:25 AM. This article is licensed under a Creative Commons Attribution 3.0 Unported Licence.

two perovskite absorbers, each presenting unique yet equally critical challenges.

From a structural perspective, monolithic 3-J architectures require interconnecting layers that simultaneously deliver high electrical conductivity and strong mechanical durability. These layers must facilitate efficient charge recombination while withstanding subsequent solution-based processing. In mechanically stacked devices, optical management becomes the dominant concern, necessitating precise control over the refractive index of intermediate layers and adhesives to minimize Fresnel reflection losses and ensure maximum light transmission. Apart from this, under real operating conditions, 3-J tandems introduce more interfaces than single-junction devices, and interface stability, particularly at organic/inorganic contacts, may become a key reliability bottleneck.

The top-cell perovskite, typically with a wide bandgap of 1.8 to 2.0 eV, is hindered by two persistent problems. First, it is highly susceptible to light-induced phase segregation, a long-standing and unresolved issue in I–Br mixed-halide systems. Second, its ultra-wide bandgap results in a high density of deep-level defects, which increase nonradiative recombination, undermine charge collection efficiency, and ultimately constrain top-cell performance.

The mid-cell perovskite faces a different but equally complex trade-off. Sn–Pb-based perovskites offer the ideal bandgap for mid-cells, yet their practical application is hindered by chemical instability, particularly the oxidation of Sn^{2+}. By contrast, $FAPbI_3$-based perovskites provide superior ambient stability and higher device efficiency, but their black α-phase remains challenging to stabilize without widening the bandgap. Achieving phase stability while maintaining optimal band alignment is therefore crucial for mid-cell perovskite optimization.

Looking ahead, the following research priorities will be central to advancing efficient and stable perovskite/perovskite/silicon 3-J solar cells: (1) improving the photostability of top-cell perovskites by eliminating light-induced phase segregation under operational conditions; (2) suppressing deep-level defect formation in wide-bandgap perovskites to reduce non-radiative losses and enhance V_{oc} and FF; (3) enhancing the chemical stability of Sn–Pb perovskites, particularly through oxidation-resistant composition design and encapsulation strategies; (4) stabilizing the black α-phase of pure $FAPbI_3$ while preserving a low bandgap near the S–Q optimum for mid-cell operation; (5) developing robust, high-conductivity interconnecting layers specifically suited for monolithic 3-J integration; (6) advancing light management strategies in mechanically stacked architectures by optimizing intermediate layers with tailored refractive index profiles.

These research directions are deeply interconnected and will require coordinated progress in material composition, interfacial engineering, and device design. Breakthroughs in these areas will not only push the solar cells' PCE beyond current records, but also accelerate the transition toward stable, scalable, and commercially viable multi-junction photovoltaic technologies.

Conflicts of interest

The authors declare no competing financial interest.

Data availability

No primary research results, software or code have been included, and no new data were generated or analyzed as part of this review.

Acknowledgements

The work is funded by KAUST under contract number ORFS-CRG12-2024-6475.

References

1 S. Rühle, *Sol. Energy*, 2016, **130**, 139–147.
2 W. Shockley and H. J. Queisser, *J. Appl. Phys.*, 1961, **32**, 510–519.
3 S. Farshad Akhtarianfar, S. Shojaei and S. Khameneh Asl, *Sol. Energy*, 2021, **220**, 70–79.
4 E. Aydin, T. G. Allen, M. De Bastiani, A. Razzaq, L. Xu, E. Ugur, J. Liu and S. De Wolf, *Science*, 2024, **383**, 1–13.
5 L. C. Hirst and N. J. Ekins-Daukes, *Prog. Photovoltaics Res. Appl.*, 2011, **19**, 286–293.
6 G. E. Eperon, M. T. Hörantner and H. J. Snaith, *Nat. Rev. Chem.*, 2017, **1**, 0095.
7 H. Li and W. Zhang, *Chem. Rev.*, 2020, **120**, 9835–9950.
8 A. De Vos, *J. Phys. D Appl. Phys.*, 1980, **13**, 839–846.
9 L. V. Mercaldo and P. D. Veneri, *Silicon Solar Cells: Materials, Technologies, Architectures*, Elsevier Ltd, 2019.
10 K. Wang, Q. Yao, J. Zhang, C. Shang, C. Li, F. Chen, T. Zhou, H. Sun, W. Zhang, H. Zhu and J. Ding, *J. Phys. Chem. C*, 2021, **125**, 23050–23057.
11 J. P. Correa-Baena, M. Saliba, T. Buonassisi, M. Grätzel, A. Abate, W. Tress and A. Hagfeldt, *Science*, 2017, **358**, 739–744.
12 Y. Rong, Y. Hu, A. Mei, H. Tan, M. I. Saidaminov, S. Il Seok, M. D. McGehee, E. H. Sargent and H. Han, *Science*, 2018, **361**(6408), eaat8235.
13 J. Y. Kim, J. W. Lee, H. S. Jung, H. Shin and N. G. Park, *Chem. Rev.*, 2020, **120**, 7867–7918.
14 P. Chen, Y. Xiao, S. Li, X. Jia, D. Luo, W. Zhang, H. J. Snaith, Q. Gong and R. Zhu, *Chem. Rev.*, 2024, **124**, 10623–10700.
15 M. A. Green, E. D. Dunlop, M. Yoshita, N. Kopidakis, K. Bothe, G. Siefer, X. Hao and J. Y. Jiang, *Prog. Photovoltaics Res. Appl.*, 2025, **33**, 795–810.
16 R. M. France, J. F. Geisz, T. Song, W. Olavarria, M. Young, A. Kibbler and M. A. Steiner, *Joule*, 2022, **6**, 1121–1135.
17 L. Xu, F. Xu, J. Liu, X. Zhang, A. S. Subbiah and S. De Wolf, *ACS Energy Lett.*, 2023, **8**, 3114–3121.
18 W. Zia, M. Malekshahi Byranvand, T. Rudolph, M. Rai, M. Kot, C. Das, M. Kedia, M. Zohdi, W. Zuo, V. Yeddu, M. I. Saidaminov, J. I. Flege, T. Kirchartz and M. Saliba, *ACS Energy Lett.*, 2024, **9**, 1017–1024.

© 2026 The Author(s). Published by the Royal Society of Chemistry

Open Access Article. Published on 04 February 2026. Downloaded on 5/20/2026 12:36:25 AM. This article is licensed under a Creative Commons Attribution 3.0 Unported Licence.

19 J. Wang, J. Peng, Y. Sun, X. Liu, Y. Chen and Z. Liang, *Adv. Electron. Mater.*, 2016, **2**, 1–6.
20 W. Liao, D. Zhao, Y. Yu, N. Shrestha, K. Ghimire, C. R. Grice, C. Wang, Y. Xiao, A. J. Cimaroli, R. J. Ellingson, N. J. Podraza, K. Zhu, R.-G. Xiong and Y. Yan, *J. Am. Chem. Soc.*, 2016, **138**, 12360–12363.
21 S. Hu, J. Thiesbrummel, J. Pascual, M. Stolterfoht, A. Wakamiya and H. J. Snaith, *Chem. Rev.*, 2024, **124**, 4079–4123.
22 J. Mei and F. Yan, *Adv. Mater.*, 2025, **37**, e2418622.
23 M. T. Hörantner, T. Leijtens, M. E. Ziffer, G. E. Eperon, M. G. Christoforo, M. D. McGehee and H. J. Snaith, *ACS Energy Lett.*, 2017, **2**, 2506–2513.
24 F. Xu, E. Aydin, I. Yavuz, C. Deger, E. Ugur, J. Liu, X. Zhang, A. Razzaq, L. Xu, M. Marengo, B. Vishal, A. Prasetio, A. Subbiah, A. Pininti, T. Allen and S. De Wolf, *Nat. Mater.*, 2026, **25**, 259–266.
25 S. Liu, Y. Lu, C. Yu, J. Li, R. Luo, R. Guo, H. Liang, X. Jia, X. Guo, Y.-D. Wang, Q. Zhou, X. Wang, S. Yang, M. Sui, P. Müller-Buschbaum and Y. Hou, *Nature*, 2024, **628**, 306–312.
26 F. Xu, E. Aydin, J. Liu, E. Ugur, G. T. Harrison, L. Xu, B. Vishal, B. K. Yildirim, M. Wang, R. Ali, A. S. Subbiah, A. Yazmaciyan, S. Zhumagali, W. Yan, Y. Gao, Z. Song, C. Li, S. Fu, B. Chen, A. ur Rehman, M. Babics, A. Razzaq, M. De Bastiani, T. G. Allen, U. Schwingenschlögl, Y. Yan, F. Laquai, E. H. Sargent and S. De Wolf, *Joule*, 2024, **8**, 224–240.
27 T. Ye, L. Qiao, T. Wang, P. Wang, L. Zhang, R. Sun, W. Kong, M. Xu, X. Yan, J. Yang, X. Zhang, L. Ma and X. Yang, *Adv. Energy Mater.*, 2024, **14**, 1–9.
28 F. Xu, J. Liu, L. Xu, A. Razzaq, X. Zhang, E. Aydin and S. De Wolf, *ACS Energy Lett.*, 2024, **9**, 3501–3504.
29 Y. J. Choi, S. Y. Lim, J. H. Park, S. G. Ji and J. Y. Kim, *ACS Energy Lett.*, 2023, **8**, 3141–3146.
30 J. Zheng, G. Wang, W. Duan, M. A. Mahmud, H. Yi, C. Xu, A. Lambertz, S. Bremner, K. Ding, S. Huang and A. W. Y. Ho-Baillie, *ACS Energy Lett.*, 2022, 3003–3005.
31 J. Werner, F. Sahli, F. Fu, J. J. Diaz Leon, A. Walter, B. A. Kamino, B. Niesen, S. Nicolay, Q. Jeangros and C. Ballif, *ACS Energy Lett.*, 2018, **3**, 2052–2058.
32 J. Zheng, G. Wang, L. Duan, W. Duan, Y. Jiang, P. Pearce, Y. Gao, M. A. Mahmud, C. Liao, T. L. Leung, J. Bing, Z. Li, Z. Sun, X. Cui, C. Bailey, M. Jankovec, J. Yi, R. Tao, L. Zheng, B. Zhu, Y. Sun, N. Sun, G. Huang, L. Wang, A. Lambertz, S. Bremner, X. Liao, T. Wu, G. Xie, M. U. Rothmann, M. Topič, D. R. McKenzie, K. Ding, W. Li, Z. Chen and A. W. Y. Ho-Baillie, *Nat. Nanotechnol.*, 2025, **20**, 1648–1655.
33 M. De Bastiani, A. S. Subbiah, E. Aydin, F. H. Isikgor, T. G. Allen and S. De Wolf, *Mater. Horiz.*, 2020, **7**, 2791–2809.
34 M. Zhang and Z. Lin, *Energy Environ. Sci.*, 2022, **15**, 3152–3170.
35 J. Lim, N.-G. Park, S. Il Seok and M. Saliba, *Energy Environ. Sci.*, 2024, **17**, 4390–4425.
36 H. Hu, S. X. An, Y. Li, S. Orooji, R. Singh, F. Schackmar, F. Laufer, Q. Jin, T. Feeney, A. Diercks, F. Gota, S. Moghadamzadeh, T. Pan, M. Rienäcker, R. Peibst, B. A. Nejand and U. W. Paetzold, *Energy Environ. Sci.*, 2024, **17**, 2800–2814.
37 F. Li, D. Wu, L. Shang, R. Xia, H. Zhang, Z. Huang, J. Gong, L. Mao, H. Zhang, Y. Sun, T. Yang, X. Sun, Z. Feng and M. Liu, *Adv. Mater.*, 2024, **36**, 1–10.
38 M. Heydarian, A. Shaji, O. Fischer, M. Günthel, O. Karalis, M. Heydarian, A. J. Bett, H. Hempel, M. Bivour, F. Schindler, M. C. Schubert, A. W. Bett, S. W. Glunz, J. Borchert and P. S. C. Schulze, *Sol. RRL*, 2025, **9**, 2400645.
39 Y. Gupta, M. Heydarian, M. Heydarian, O. Er-raji, M. Günthel, O. Fischer, C. Baretzky, P. S. C. Schulze, M. Bivour, S. De Wolf, S. W. Glunz and J. Borchert, *Prog. Photovoltaics Res. Appl.*, 2025, **33**, 782–794.
40 M. Heydarian, M. Heydarian, A. J. Bett, M. Bivour, F. Schindler, M. Hermle, M. C. Schubert, P. S. C. Schulze, J. Borchert and S. W. Glunz, *ACS Energy Lett.*, 2023, **8**, 4186–4192.
41 J. Song, H. Xie, E. L. Lim, A. Hagfeldt and D. Bi, *Adv. Energy Mater.*, 2022, **12**, 1–38.
42 J. Tian, Q. Xue, Q. Yao, N. Li, C. J. Brabec and H. Yip, *Adv. Energy Mater.*, 2020, **10**, 1–28.
43 Q. Zeng, X. Zhang, C. Liu, T. Feng, Z. Chen, W. Zhang, W. Zheng, H. Zhang and B. Yang, *Sol. RRL*, 2019, **3**, 1–17.
44 Q. Tai, K.-C. Tang and F. Yan, *Energy Environ. Sci.*, 2019, **12**, 2375–2405.
45 A. Kiligaridis, P. A. Frantsuzov, A. Yangui, S. Seth, J. Li, Q. An, Y. Vaynzof and I. G. Scheblykin, *Nat. Commun.*, 2021, **12**, 3329.
46 L. A. Muscarella and B. Ehrler, *Joule*, 2022, **6**, 2016–2031.
47 R. A. Kerner, Z. Xu, B. W. Larson and B. P. Rand, *Joule*, 2021, **5**, 2273–2295.
48 X. Tang, M. Van Den Berg, E. Gu, A. Horneber, G. J. Matt, A. Osvet, A. J. Meixner, D. Zhang and C. J. Brabec, *Nano Lett.*, 2018, **18**, 2172–2178.
49 D. J. Slotcavage, H. I. Karunadasa and M. D. McGehee, *ACS Energy Lett.*, 2016, **1**, 1199–1205.
50 A. J. Knight and L. M. Herz, *Energy Environ. Sci.*, 2020, **13**, 2024–2046.
51 G. E. Eperon, T. Leijtens, K. A. Bush, R. Prasanna, T. Green, J. T.-W. Wang, D. P. McMeekin, G. Volonakis, R. L. Milot, R. May, A. Palmstrom, D. J. Slotcavage, R. A. Belisle, J. B. Patel, E. S. Parrott, R. J. Sutton, W. Ma, F. Moghadam, B. Conings, A. Babayigit, H.-G. Boyen, S. Bent, F. Giustino, L. M. Herz, M. B. Johnston, M. D. McGehee and H. J. Snaith, *Science*, 2016, **354**, 861–865.
52 Z. Yang, Z. Yu, H. Wei, X. Xiao, Z. Ni, B. Chen, Y. Deng, S. N. Habisreutinger, X. Chen, K. Wang, J. Zhao, P. N. Rudd, J. J. Berry, M. C. Beard and J. Huang, *Nat. Commun.*, 2019, **10**, 4498.
53 L. Chen, J. W. Yoo, M. Hu, S. Lee and S. Il Seok, *Angew. Chem., Int. Ed.*, 2022, **61**, 1–7.
54 L. Lanzetta, T. Webb, N. Zibouche, X. Liang, D. Ding, G. Min, R. J. E. Westbrook, B. Gaggio, T. J. Macdonald, M. S. Islam and S. A. Haque, *Nat. Commun.*, 2021, **12**, 2853.
55 H. Yuan, X. Li, W. Zhang, Y. Hu, J. Xu, T. You, Q. Weng, Y. Mao, T. Shu and J. Fang, *Adv. Mater.*, 2025, **37**, 1–10.

© 2026 The Author(s). Published by the Royal Society of Chemistry

Open Access Article. Published on 04 February 2026. Downloaded on 5/20/2026 12:36:25 AM.
This article is licensed under a Creative Commons Attribution 3.0 Unported Licence.

56 M. Yang, Y. Bai, Y. Meng, R. Tian, K. Sun, X. Lu, H. Pan, J. Wang, S. Zhou, J. Zhang, Z. Song, Y. Wang, C. Liu and Z. Ge, *Adv. Mater.*, 2025, **37**, 1–10.
57 Y. Bai, R. Tian, K. Sun, C. Liu, X. Lang, M. Yang, Y. Meng, C. Xiao, Y. Wang, X. Lu, J. Wang, H. Pan, Z. Song, S. Zhou and Z. Ge, *Energy Environ. Sci.*, 2024, **17**, 8557–8569.
58 R. Wang, T. Huang, J. Xue, J. Tong, K. Zhu and Y. Yang, *Nat. Photonics*, 2021, **15**, 411–425.
59 J. Lim, N.-G. Park, S. Il Seok and M. Saliba, *Energy Environ. Sci.*, 2024, **17**, 4390–4425.
60 J.-P. Connerade, *AIP Conf. Proc.*, 2009, **1197**, 1–33.
61 H. Zhang and N.-G. Park, *Angew. Chem., Int. Ed.*, 2022, **61**, e202212268.
62 H. Min, M. Kim, S.-U. Lee, H. Kim, G. Kim, K. Choi, J. H. Lee and S. Il Seok, *Science*, 2019, **366**, 749–753.
63 X. Liu, D. Luo, Z.-H. Lu, J. S. Yun, M. Saliba, S. Il Seok and W. Zhang, *Nat. Rev. Chem.*, 2023, **7**, 462–479.
64 H.-S. Kim, J.-W. Lee, A. Hagfeldt, M. Grätzel and N.-G. Park, *Chem. Soc. Rev.*, 2025, **54**, 11061–11088.
65 B. Park and S. Il Seok, *Adv. Mater.*, 2019, **31**, 1–17.

© 2026 The Author(s). Published by the Royal Society of Chemistry